

Near-optimality of conservative driving in discrete systems

Jann van der Meer* and Andreas Dechant†

Department of Physics No. 1, Graduate School of Science, Kyoto University, Kyoto 606-8502, Japan

(Dated: February 23, 2026)

Transferring a physical system from an initial to a final state while minimizing energetic losses is an interdisciplinary control problem that bridges stochastic thermodynamics and optimal transport theory. Recent research typically considers problems in which the optimal solution is realized via conservative forces, but whether this situation applies depends on the problem's constraints. In systems with complex topologies like discrete networks, the optimal, dissipation-minimizing protocol involves applying nonconservative forces along cycles if the timescales of the transitions in the network are fixed. We show that although nonconservative driving is optimal in this setting, a conservative protocol exists whose dissipation is at most twice the optimal one. This finding is complemented with an example modeling transport across an energy barrier, which illustrates such improvements of order 1 explicitly. Qualitatively, conservative driving falls short of achieving optimality because direct transport across the barrier is avoided. We conclude with a discussion that the optimality of nonconservative driving might be a generic phenomenon: As fewer degrees of freedom can be optimized, additional degrees of freedom due to adding nonconservative forces become more significant.

Introduction— Optimizing physical systems to minimize their dissipation is of practical importance for the design of energy-efficient devices. It is therefore crucial to understand the mechanisms that cause dissipation and to discover general strategies to reduce it. One approach to tackling these issues is the framework of optimal transport [1–3], whose goal is to achieve a desired outcome while minimizing a cost function. When the cost function is taken to be the entropy production of a physical process, the result are optimal physical forces that allow realizing the process with minimal dissipation [4–8]. While the concrete optimal forces can often only be computed approximately, in many cases the optimal forces can be shown to be conservative [4, 7, 9], which reduces the optimization problem to the construction of an optimal potential function.

From a physical point of view, nonconservative forces prevent a system from relaxing to an equilibrium state and are themselves a source of dissipation [10–15]. However, from the point of view of optimization, conservative forces are merely a tiny subset of all possible forces, thus it is surprising that optimizing over the much larger space of nonconservative forces does not improve the result. Indeed, nonconservative forces enable new phenomena or improve performance in various artificial and biological systems, such as anomalous relaxation [16, 17], autonomous feedback [18], coherent oscillations [19, 20], cooling [21], collective phenomena in active matter [22, 23], enhanced sensing [24], sensory adaption [25], signal transduction [26] and optimal driving in viscous media [27].

One exception to the optimality of conservative forces was discovered in Ref. [28]: In discrete jump processes, the optimal forces minimizing the entropy production rate are generally nonconservative. This result can be reconciled with other findings [7, 9, 15, 29, 30] by noting that, for jump processes, minimizing dissipation leads to

a non-trivial solution only under additional constraints [9, 31]. These constraints represent the physical reality that transitions between different states cannot occur arbitrarily fast; whether the optimal forces are conservative or not depends on the precise constraints. Constraints, such as on the magnitude of transition rates or forces are also ubiquitous in practical applications, where they may prohibit us from realizing the solution prescribed by optimal transport theory. Even though the latter may be conservative, the optimal forces under the relevant physical constraints may be nonconservative.

This raises two key questions: First, how can we understand the conditions under which the optimal forces are nonconservative and how can they reduce dissipation compared to conservative forces? Second, how much can dissipation be reduced by nonconservative forces and are conservative forces still near-optimal?

In this Letter, we address these questions on the background of Refs. [28, 31]. We consider a Markov jump process on a discrete state space, and minimize the entropy production for a given initial and final state, under the constraint that the symmetric part of the transition rates is fixed. We show that, under these conditions, the optimal nonconservative forces can reduce the entropy production at most by a factor of 2 compared to conservative forces. In that sense, conservative forces are near-optimal, resulting in a dissipation less than twice the minimal possible amount. Moreover, we construct and explicitly optimize a one-dimensional model consisting of a ring with a single large energy barrier. We show that the optimality of nonconservative forces can be attributed to their greater flexibility, allowing to precisely balance the probability flow across the barrier and through the bulk of the ring.

Minimal dissipation in discrete systems— For a Markovian dynamics on a set of N discrete states, the probability of finding the system in state i , $p_i(t)$, evolves

according to the master equation

$$-\dot{p}_i(t) = \sum_{j \neq i} j_{ij}(t) = \sum_{j \neq i} [p_i(t)k_{ij}(t) - p_j(t)k_{ji}(t)], \quad (1)$$

a continuity equation that describes that a change of probability in state i must be due to a current $j_{ij}(t)$ to a neighboring state j . The current can also be expressed in terms of $p_i(t)$ and $k_{ij}(t)$, the rate of transitions to state j if the system is in state i at time t . From the perspective of optimal transport problems, the master equation (1) encodes constraints on every possible transport plan imposed by the system's topological features.

In addition to fixing the topology, the transport problem of moving probability between two states requires specifying the cost function to be optimized. In the context of thermodynamics, a natural and physically well-motivated cost term is given by the total entropy production $S = \int_0^T \sigma dt$ between two specified times 0 and T . The integrand

$$\sigma = \sum_{i,j} p_i(t)k_{ij}(t) \ln \frac{p_i(t)k_{ij}(t)}{p_j(t)k_{ji}(t)} \quad (2)$$

is the instantaneous entropy production rate in units of Boltzmann's constant $k_B = 1$ [10, 32]. Without any additional constraints, infinitely fast but almost symmetric transitions allow transporting probability with vanishing entropy production, thereby trivializing the optimization problem [31]. We can fix the timescale of the transitions in the system by parameterizing the transition rates as [28, 31, 32]

$$k_{ij}(t) = \kappa_{ij}(t)e^{A_{ij}(t)/2} \quad (3)$$

with a nonnegative symmetric matrix $\kappa_{ij}(t) = \kappa_{ji}(t) \geq 0$, and an antisymmetric matrix $A_{ij}(t) = -A_{ji}(t)$. This parametrization has a clear thermodynamic interpretation: The antisymmetric part $A_{ij}(t)$ models the forces in the system, whereas the symmetric part encodes kinetic information, e.g., the presence of energy barriers between states and the connectivity of the state space. We say that two states i and j are connected when $\kappa_{ij}(t) > 0$, which we interpret as an edge in the graph whose vertices are the states i .

Assuming that we can control the forces in the system, optimizing $A_{ij}(t)$, whereas $\kappa_{ij}(t)$ remains fixed, results in a nontrivial optimization problem in which the entropy production rate takes the form

$$\sigma = \sum_{i,j} \omega_{ij}(t) F_{ij}(t) \sinh \frac{F_{ij}(t)}{2}. \quad (4)$$

The symmetric matrix $\omega_{ij}(t) := \kappa_{ij}(t)\sqrt{p_i(t)p_j(t)}$ quantifies the timescale of the rate of transitions between states i and j . For an equilibrium system, $\omega_{ij}(t)$ coincides with the traffic. The expression (4) is convex in the

thermodynamic forces

$$F_{ij}(t) := A_{ij}(t) + \ln(p_i(t)/p_j(t)) = 2 \operatorname{asinh} \frac{j_{ij}(t)}{2\omega_{ij}(t)}, \quad (5)$$

and the system is in equilibrium if and only if $F_{ij}(t) = 0$ for every pair of states for which $\omega_{ij}(t) > 0$. We say that the forces in the system are conservative if a state function $\psi_i(t)$ exists such that $F_{ij}(t) = \psi_i(t) - \psi_j(t)$, which is equivalent to $A_{ij}(t) = \phi_i(t) - \phi_j(t)$ with $\phi_i(t) = \psi_i(t) - \ln(p_i(t))$.

Being able to change $A_{ij}(t)$ is equivalent to being able to control $F_{ij}(t)$ or the current $j_{ij}(t)$ at each transition. Optimizing over $F_{ij}(t)$ (M degrees of freedom (DOF) if the graph has M edges) can be reparametrized and equivalently understood as an optimization over all $\dot{p}_i(t)$ ($N-1$ DOF for an N -state system), followed by a constrained optimization over all cycle currents ($C = M - (N-1)$ DOF for a system with C fundamental cycles). This latter optimization over currents j_C along a cycle C corresponds to adjusting circular flows in the network and can be performed for fixed $\dot{p}_i(t)$, i.e., without affecting the time-evolution of the system, by taking the derivative with respect to a cycle current ∂_{j_C} as explained in Appendix A.

Therefore, and because entropy production is additive in a Markovian system, the optimization over the cycle currents j_C can be performed independently for each point in time t . Thus, we can consider a fixed point in time t and suppress the time arguments. Minimizing the entropy production rate then corresponds to the condition

$$\partial_{j_C} \sigma = 2 \sum_{(ij) \in C} (\tanh(F_{ij}/2) + F_{ij}/2) = 0. \quad (6)$$

On the other hand, for conservative forces $F_{ij} = \psi_i - \psi_j$, the cycle affinity

$$\mathcal{A}_C = \sum_{(ij) \in C} F_{ij} = \sum_{(ij) \in C} A_{ij}. \quad (7)$$

vanishes for any cycle C . Comparing (6) and (7), we see that, surprisingly, the conditions for minimal entropy production and vanishing cycle affinity are different and, thus, optimal driving generally requires nonconservative forces.

Conflicting intuitions— This perhaps surprising insight leaves us with at first glance contradictory perspectives. On the one hand, nonconservative driving generates cycle currents that generally increase dissipation, which prompts the question how nonconservative driving can be optimal. On the other hand, the same cycle currents correspond to additional optimizable degrees of freedom enabled by nonconservative driving forces, in turn provoking the question why conservative driving is optimal in many previously studied situations, e.g., for

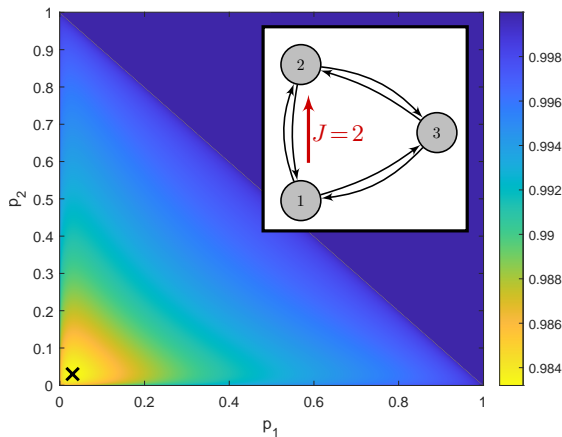


FIG. 1. Optimal versus conservative driving in a three-state Markov network. Colors encode the maximal possible improvement $\sigma^*/\sigma^{\text{cons.}}$ according to the color scale. For given occupation probabilities p_i , the configurations that yield a desired current $J = \dot{p}_2 = -\dot{p}_1$ can be parametrized by the cycle affinity $\mathcal{A} = A_{12} + A_{23} + A_{31}$. The minimal thermodynamic cost (2) σ^* after optimizing \mathcal{A} is compared to the cost $\sigma^{\text{cons.}}$ of the conservative protocol satisfying $A_{12} + A_{23} + A_{31} = 0$. The transition rates are parametrized as in Eq. (3) with fixed $\kappa_{ij} = 1$ for $i \neq j$. For $J = 2$, the minimum $\sigma^*/\sigma^{\text{cons.}} = 0.983$ is located at $(p_1, p_2) = (0.03, 0.03)$.

constant activity [9, 30], slow driving [29] and in the continuum limit [9, 28]. How can we reconcile these seemingly contradictory viewpoints? More practically, how do we find situations in which additional nonconservative forces offer significant improvement?

A first insight is that discrepancies between Eqs. (6) and (7) are only observed at order $\mathcal{O}(F_{ij}^3)$, implying that the optimal and conservative protocol coincide near equilibrium. However, a naive far-from-equilibrium limit is not helpful either: Devising a large F_{ij} , e.g., via the limit of vanishing occupation probability for a single state j , $p_j \rightarrow 0$, leads to a diverging entropy production rate, but this divergence is independent of the cycle currents. Thus, adding nonconservative forces provides no benefit in this limit. In a numerical case study [28], the improvement of optimal nonconservative over conservative protocols has been reported to be of a relative magnitude of $\sim 10^{-2}$, which is also confirmed by optimizing over the possible probabilities p_i in a three-state system in Fig. 1. Even when focusing on the nonadiabatic entropy production [32, 33], i.e., when disregarding the cost of the stationary cycle current, a numerical case study shows limited improvements that vanish in both limits of slow and fast driving [34]. What is lacking is a way to systematically access and bound the difference between the costs of the conservative and optimal protocol. This is the purpose of the following main result.

Main result— We define

$$\rho = \sum_{i,j} \omega_{ij} C(F_{ij}) \quad (8)$$

with $C(x) = x \sinh(x/2) - 2[\cosh(x/2) - 1]$. Like σ , ρ is a convex measure of distance to equilibrium, which additionally satisfies $\sigma/2 \leq \rho \leq \sigma$, because $C(x) \geq (x/2) \sinh(x/2)$. The thermodynamic interpretation and properties of ρ will be discussed in detail in an upcoming publication [35]. Here, we only use the property that ρ is minimized by conservative forces, which is derived below. This provides a quantitative way to compare optimal and conservative transport. At each point in time t , the minimal entropy production rate σ^* associated with the optimal protocol bounds the entropy production rate $\sigma^{\text{cons.}}$ of the corresponding conservative protocol with the same time evolution from above and below,

$$\sigma^* \leq \sigma^{\text{cons.}} \leq 2\sigma^*, \quad (9)$$

which can be derived from $\sigma/2 \leq \rho \leq \sigma$ as shown in Appendix B. By integrating over the duration T of a protocol, we obtain bounds on the total entropy production $S^* := \int_0^T \sigma^* dt$ of the optimal protocol

$$\frac{S^{\text{cons.}}}{2} \leq S^* \leq S^{\text{cons.}} := \int_0^T \sigma^{\text{cons.}} dt. \quad (10)$$

This relation establishes that conservative protocols, while not necessarily optimal, are near-optimal in the sense that deviations from the optimal solution are bounded by the constant numerical factor of 2. In other words, given an optimal transport problem, conservative forces provide a sensible trial solution whose cost can be reduced by at most half.

An illustrating example— Next, we construct an explicit example in which optimal and conservative driving show distinctly different behavior. We assume a uniform probability distribution $p_i = 1/N$ over N states arranged in a cycle. The symmetric part of the transition rates for two neighboring states i, j is specified as

$$N\omega_{ij} = \kappa_{ij} = \begin{cases} e^{-E_b} & i = 1, j = 2 \text{ or } i = 2, j = 1 \\ 1 & \text{else, if connected} \end{cases}, \quad (11)$$

modeling an energy barrier $E_b > 0$ between states 1 and 2, cf. Fig. 2 a). The energy barrier incorporates the numerical insight of Fig. 1 that the best results are achieved if probability is to be transported across transition with a “slow” timescale $\omega_{12} = \kappa_{12}\sqrt{p_1 p_2}$. While the previous numerical optimization achieved this via small occupation probabilities p_1, p_2 , adjusting κ_{12} directly allows control over this timescale without modifying p_i .

Transporting probability at the rate $J/N = \dot{p}_2 = -\dot{p}_1$ from state 1 to 2 can be achieved either through a local force A_{12} that directly affects the current j_{12} across the

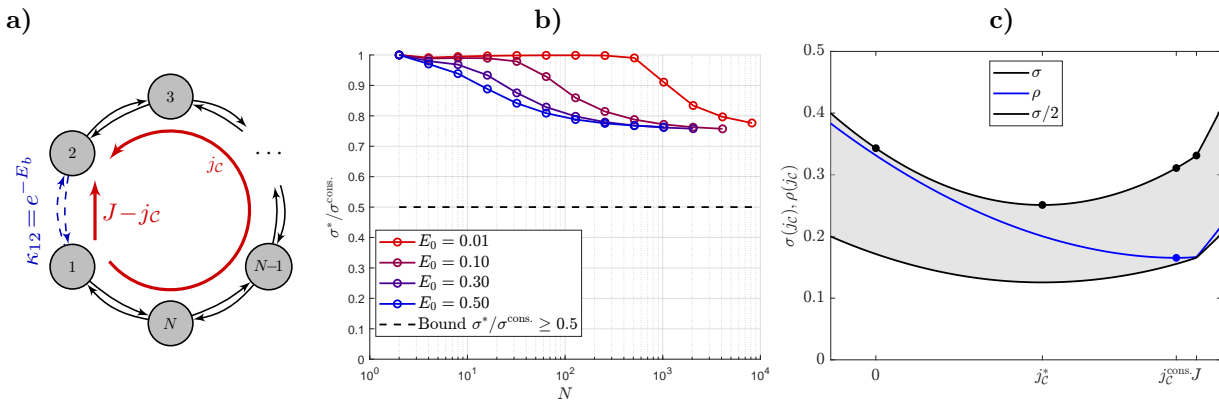


FIG. 2. Transport across an energy barrier in a unicyclic network. a) Set-up: The transitions' timescales are $\kappa_{12} = e^{-E_b}$, modeling an energy barrier of height $E_b = NE_0$, and $\kappa_{ij} = 1$ otherwise. A desired change in probability $\dot{p}_2 = -\dot{p}_1 = J$ can be accomplished through a local current j_{12} across the energy barrier or a cycle current $j_c = J - j_{12}$ through the bulk. b) Comparison of conservative and optimal transport with respective costs σ^* and $\sigma^{\text{cons.}}$. The theoretical lower bound $\sigma^*/\sigma^{\text{cons.}} \geq 0.5$ (cf. Eq. (9)) is compared to numerical calculations for $p_i = 1/N$ and optimized J . Increasing N leads to a decrease in $\sigma^*/\sigma^{\text{cons.}}$, but becomes increasingly numerically unstable. A minimal value of $\sigma^*/\sigma^{\text{cons.}} \simeq 0.76$ can be attained for various values of E_0 . c) Entropy production $\sigma(j_c)$ and $\rho(j_c)$ (cf. Eq. (8)) as a function of the bulk current j_c for $N = 100$, $E_0 = 0.3$ and the numerically optimized $J \simeq 0.58$. The optimal solution $j_c^* \simeq 0.3$ balances transport across the energy barrier and through the bulk. In contrast, the conservative solution $j_c^{\text{cons.}} \simeq 0.55$ minimizes ρ (cf. Eq. (13)) and mostly transports current through the bulk.

energy barrier or by transporting probability through the bulk of the cycle, which we parametrize as $j_c/N = J/N - j_{12}$. Using Eqs. (4) and (5), the entropy production rate

$$\sigma = \frac{2(N-1)}{N} j_c \operatorname{asinh} \frac{j_c}{2} + \frac{2}{N} (J - j_c) \operatorname{asinh} \frac{J - j_c}{2e^{-E_b}} \quad (12)$$

can be optimized as a function of j_c . The minimizer j_c^* can be contrasted with $j_c^{\text{cons.}}$, the value of j_c that solves $0 = 2(N-1)\operatorname{asinh}(j_c/2) - 2\operatorname{asinh}([J - j_c]/2e^{-E_b})$ and therefore indicates conservative driving (cf. Eq. (7) and Appendix D for details). For large N and suitably scaled $E_b = NE_0$ with constant E_0 , the solutions j_c^* and $j_c^{\text{cons.}}$ show different qualitative behavior. The numerical calculation in Fig. 2b) indicates a ratio of up to $\sigma^*/\sigma^{\text{cons.}} \simeq 0.76$, yielding an improvement of about $\sim 32\%$ for optimal over conservative driving. Qualitatively, an explicit illustration of Eq. (12) in Fig. 2c) reveals that the optimal current j_c^* balances transport through the bulk with transport across the barrier, whereas the larger $j_c^{\text{cons.}}$ indicates that transport through the barrier is mostly avoided. For larger N , this effect becomes more pronounced, as illustrated in Appendix D.

Conservative protocols minimize ρ — Like the entropy production rate, ρ measures how far the system is from equilibrium. Asking for the dynamics that minimizes ρ for a given time evolution corresponds to minimizing (8) with respect to F_{ij} under the constraint (1). As discussed earlier for the entropy production rate, this problem is equivalent to minimizing ρ with respect to the cycle currents j_c of each fundamental cycle \mathcal{C} in the system. An explicit calculation (see Appendix C) results in

a condition on the optimal parameters F_{ij} ,

$$0 = \partial_{j_c} \rho = \sum_{(ij) \in \mathcal{C}} F_{ij}, \quad (13)$$

which is precisely the condition (7) of vanishing cycle affinities. This finding implies that the optimal thermodynamic forces F_{ij}^* can be written as the difference of a state function ψ_i ,

$$F_{ij}^* = \psi_i - \psi_j. \quad (14)$$

Thus, we find that, in contrast to the entropy production rate, the force minimizing ρ is conservative.

Discussion and outlook— Model classes in which nonconservative driving is optimal are less explored than scenarios in which conservative driving can achieve optimality. Our results show that properties of the optimal solution depend crucially on a problem's constraints, e.g., which parameters are fixed and which can be optimized. It is expected that the fewer DOF available for optimization, the more significant the additional DOF gained through nonconservative driving become. This suggests that, rather than being an exception, optimality of nonconservative driving may be the generic case in real-world scenarios involving manifold and complex constraints.

A concrete comparison can be drawn between this work and Ref. [9]: Both consider the same optimization problem in a discrete system, but for different constraints. In this work, the symmetric part κ_{ij} is fixed for all times and individually for each transition, whereas in Ref. [9]

the total activity, either at each point in time or its integral, is fixed. Intuitively, the latter condition is looser. At each point in time, only the overall timescale rather than the timescale of each individual transition is fixed, thus nonconservative effects, which require a nontrivial topology, can be effectively “turned off” by making one transition in a cycle arbitrarily slow. The stronger constraints in the set-up of this work prevent this effect, therefore a reduction to an effectively tree-like network is not possible. Nonconservative forces are then needed to adapt to the topologically nontrivial situation.

The mutable nature of optimal solutions depending on their constraints stimulates a shift in attention in problems of minimal cost towards the constraints themselves. The parametrization of rates adapted in this work is not unique but can, e.g., be generalized to different splittings between symmetric and antisymmetric parts (i.e., different load-sharing factors [36–38]) or even further to general nonlinear relationships between control parameters and transition rates. To explore this vast realm of possible system classes, it is also worthwhile to investigate the microscopic origin of possible rate parameterizations. A theoretical starting point is to coarse-grain a Langevin model of, say, a bistable or tilted potential under the presence of a control parameter for the driving, and then investigate the rate parameterizations emerging in an effective discrete Markovian approximation. Another question of interest is whether the theoretical bound $\sigma^*/\sigma^{\text{cons.}} \geq 1/2$ can be attained by an explicit model, or whether a tighter bound exists. We leave the investigation of such stronger bounds as an open problem for future work.

Acknowledgments— JvdM was supported by JSPS KAKENHI (Grants No. 24H00833 and 25KF0238) and JSPS Research Fellowship No. P25761. AD was supported by JSPS KAKENHI (Grants No. 22K13974, 24H00833 and 25K00926). This work was supported by JST ERATO Grant Number JPMJER2302, Japan.

* vandermeer.jann.57d@st.kyoto-u.ac.jp

† andreas.dechant@outlook.com

- [1] G. Monge, *Memoire sur la theorie des deblais et des remblais*, *Histoire de l’Academie Royale des Sciences de Paris* (1781).
- [2] J.-D. Benamou and Y. Brenier, A computational fluid mechanics solution to the Monge-Kantorovich mass transfer problem, *Numer. Math.* **84**, 375 (2000).
- [3] C. Villani, *Optimal Transport: Old and New*, Grundlehren der mathematischen Wissenschaften (Springer Berlin Heidelberg, 2008).
- [4] E. Aurell, C. Mejía-Monasterio, and P. Muratore-Ginanneschi, Optimal Protocols and Optimal Transport in Stochastic Thermodynamics, *Physical Review Letters* **106**, 250601 (2011).
- [5] E. Aurell, K. Gawędzki, C. Mejía-Monasterio, R. Mohayae, and P. Muratore-Ginanneschi, Refined Second Law of Thermodynamics for Fast Random Processes, *Journal of Statistical Physics* **147**, 487 (2012).
- [6] M. Nakazato and S. Ito, Geometrical aspects of entropy production in stochastic thermodynamics based on Wasserstein distance, *Phys. Rev. Research* **3**, 043093 (2021).
- [7] T. Van Vu and K. Saito, Thermodynamic Unification of Optimal Transport: Thermodynamic Uncertainty Relation, Minimum Dissipation, and Thermodynamic Speed Limits, *Physical Review X* **13**, 011013 (2023).
- [8] S. Oikawa, Y. Nakayama, S. Ito, T. Sagawa, and S. Toyabe, Experimentally achieving minimal dissipation via thermodynamically optimal transport, *Nature Communications* **16**, 10424 (2025).
- [9] A. Dechant, Minimum entropy production, detailed balance and Wasserstein distance for continuous-time Markov processes, *Journal of Physics A: Mathematical and Theoretical* **55**, 094001 (2022).
- [10] J. Schnakenberg, Network theory of microscopic and macroscopic behavior of master equation systems, *Reviews of Modern Physics* **48**, 571 (1976).
- [11] T. L. Hill, *Free Energy Transduction and Biochemical Cycle Kinetics* (Springer New York, 1989).
- [12] T. Hatano and S.-i. Sasa, Steady-state thermodynamics of Langevin systems, *Phys. Rev. Lett.* **86**, 3463 (2001).
- [13] C. Maes and K. Netočný, Minimum entropy production principle from a dynamical fluctuation law, *J. Math. Phys.* **48**, 053306 (2007).
- [14] A. Dechant, S.-i. Sasa, and S. Ito, Geometric decomposition of entropy production in out-of-equilibrium systems, *Phys. Rev. Research* **4**, L012034 (2022).
- [15] K. Yoshimura, A. Kolchinsky, A. Dechant, and S. Ito, Housekeeping and excess entropy production for general nonlinear dynamics, *Physical Review Research* **5**, 013017 (2023).
- [16] J. Degünther and U. Seifert, Anomalous relaxation from a non-equilibrium steady state: An isothermal analog of the Mpemba effect, *Europhysics Letters* **139**, 41002 (2022).
- [17] C. Dieball, G. Wellecke, and A. Godec, Asymmetric thermal relaxation in driven systems: Rotations go opposite ways, *Physical Review Research* **5**, L042030 (2023).
- [18] P. Strasberg, G. Schaller, T. Brandes, and M. Esposito, Thermodynamics of a Physical Model Implementing a Maxwell Demon, *Physical Review Letters* **110**, 040601 (2013).
- [19] A. C. Barato and U. Seifert, Coherence of biochemical oscillations is bounded by driving force and network topology, *Physical Review E* **95**, 062409 (2017).
- [20] N. Ohga, S. Ito, and A. Kolchinsky, Thermodynamic Bound on the Asymmetry of Cross-Correlations, *Physical Review Letters* **131**, 077101 (2023).
- [21] S. A. M. Loos and S. H. L. Klapp, Irreversibility, heat and information flows induced by non-reciprocal interactions, *New Journal of Physics* **22**, 123051 (2020).
- [22] M. Knežević, T. Welker, and H. Stark, Collective motion of active particles exhibiting non-reciprocal orientational interactions, *Scientific Reports* **12**, 19437 (2022).
- [23] É. Fodor, R. L. Jack, and M. E. Cates, Irreversibility and Biased Ensembles in Active Matter: Insights from Stochastic Thermodynamics, *Annual Review of Con-*

- densed Matter Physics **13**, 215 (2022).
- [24] A. Dechant and E. Lutz, Fundamental limits on nonequilibrium sensing, *Nature Communications* **16**, 10227 (2025).
 - [25] G. Lan, P. Sartori, S. Neumann, V. Sourjik, and Y. Tu, The energy–speed–accuracy trade-off in sensory adaptation, *Nature physics* **8**, 422 (2012).
 - [26] S. Ito and T. Sagawa, Maxwell’s demon in biochemical signal transduction with feedback loop, *Nature Communications* **6**, 7498 (2015).
 - [27] S. A. M. Loos, S. Monter, F. Ginot, and C. Bechinger, Universal Symmetry of Optimal Control at the Microscale, *Physical Review X* **14**, 021032 (2024).
 - [28] B. Remlein and U. Seifert, Optimality of nonconservative driving for finite-time processes with discrete states, *Physical Review E* **103**, L050105 (2021).
 - [29] E. Ilker, Ö. Güngör, B. Kuznets-Speck, J. Chiel, S. Deffner, and M. Hinczewski, Shortcuts in Stochastic Systems and Control of Biophysical Processes, *Physical Review X* **12**, 021048 (2022).
 - [30] R. Nagayama, K. Yoshimura, and S. Ito, Infinite variety of thermodynamic speed limits with general activities, *Physical Review Research* **7**, 013307 (2025).
 - [31] P. Muratore-Ginanneschi, C. Mejía-Monasterio, and L. Peliti, Heat Release by Controlled Continuous-Time Markov Jump Processes, *Journal of Statistical Physics* **150**, 181 (2013).
 - [32] U. Seifert, *Stochastic thermodynamics* (Cambridge University Press, Cambridge, England, 2025).
 - [33] M. Esposito and C. Van Den Broeck, Three Detailed Fluctuation Theorems, *Physical Review Letters* **104**, 090601 (2010).
 - [34] J.-C. Delvenne and G. Falasco, Thermokinetic relations, *Physical Review E* **109**, 014109 (2024).
 - [35] A. Dechant and J. Van der Meer, In preparation.
 - [36] M. E. Fisher and A. B. Kolomeisky, Molecular motors and the forces they exert, *Physica A: Statistical Mechanics and its Applications* **274**, 241 (1999).
 - [37] A. B. Kolomeisky and M. E. Fisher, Molecular Motors: A Theorist’s Perspective, *Annual Review of Physical Chemistry* **58**, 675 (2007).
 - [38] E. Zimmermann and U. Seifert, Efficiencies of a molecular motor: A generic hybrid model applied to the F₁-ATPase, *New Journal of Physics* **14**, 103023 (2012).

END MATTER

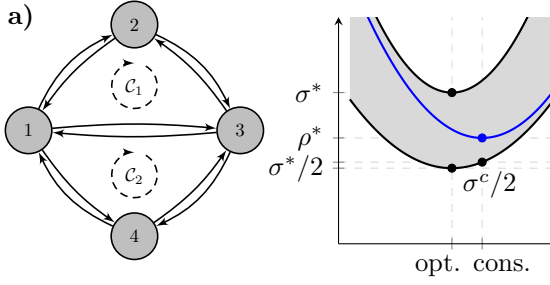


FIG. 3. a) A Markov network with two fundamental cycles $\mathcal{C}_1 = (1231)$ and $\mathcal{C}_2 = (1341)$. In this example, $\partial_{j_{\mathcal{C}_1}} = \partial_{j_{12}} + \partial_{j_{23}} - \partial_{j_{13}}$. Note that increasing the cycle currents $j_{12}, j_{13}, j_{31} = -j_{13}$ by the same amount does not affect a given time evolution of the occupation probabilities $p_i(t)$. b) Visualization of the derivation that a relation $\sigma/2 \leq \rho \leq \sigma$ between two cost functions σ, ρ implies the same chain of inequalities on their minimal values σ^*, ρ^* . We can relate σ^c , the value of σ evaluated at the point at which ρ is minimized, to its minimum σ^* via $\sigma^c \leq 2\sigma^*$. In the main text, the configurations minimizing σ and ρ characterize optimal and conservative driving, respectively.

Appendix A: Cycles and cycle currents— The time evolution of the probabilities $p_i(t)$ for all times t according to Eq. (1) does not determine the time evolution of the currents $j_{ij}(t)$ from state i to j if the system's topology is nontrivial and contains cycles. The remaining degrees of freedom are specified by the cycle currents on a set of fundamental cycles [10], which form a basis for all possible cycles (cf. Fig. 3a) for an example). We understand a cycle \mathcal{C} as a path (a sequence of directed edges) in the network that enters a state at most once and whose first and last state coincide, forming a closed loop. We write $(ij) \in \mathcal{C}$ if the transition $i \rightarrow j$ is contained in \mathcal{C} . The directed adjacency matrix of a cycle \mathcal{C} is defined as

$$\chi_{ij}^{\mathcal{C}} = \begin{cases} 1 & \text{if } i \rightarrow j \text{ is contained in } \mathcal{C} \\ -1 & \text{if } j \rightarrow i \text{ is contained in } \mathcal{C} \\ 0 & \text{otherwise} \end{cases}, \quad (15)$$

which enables us to rigorously define the derivative with respect to the cycle current $\partial_{j_{\mathcal{C}}}$ as

$$\partial_{j_{\mathcal{C}}} = \sum_{(ij) \in \mathcal{C}} \partial_{j_{ij}} = \sum_{i < j} \chi_{ij}^{\mathcal{C}} \partial_{j_{ij}} = \frac{1}{2} \sum_{ij} \chi_{ij}^{\mathcal{C}} \partial_{j_{ij}}, \quad (16)$$

where $i < j$ ensures that each edge is contained exactly once in the sum. The decomposition of cycles into fundamental cycles (e.g. $\mathcal{C} = \mathcal{C}_1 + \mathcal{C}_2$) translates into a corresponding linear combination of differential operators (e.g. $\partial_{j_{\mathcal{C}}} = \partial_{j_{\mathcal{C}_1}} + \partial_{j_{\mathcal{C}_2}}$

Appendix B: Bounds on cost functions imply bounds on their minima— We consider two cost functions $\sigma(x), \rho(x)$ on the same domain satisfying

$$\sigma/2 \leq \rho \leq \sigma \quad (17)$$

and denote their respective minima as σ^* and ρ^* . For x_c , defined as the x -value minimizing ρ , we have $\sigma^* \leq \sigma^c := \sigma(x_c) \leq 2\rho^*$ by virtue of the first inequality in (17). For x_o , the x -value that minimizes σ , we have $\rho^* \leq \rho(x_o) \leq \sigma(x_o) = \sigma^*$, where the second inequality makes use of (17). Combining these two relations, we obtain

$$\sigma^* \leq \sigma^c \leq 2\rho^* \leq 2\sigma^*, \quad (18)$$

which includes the finding $\sigma^c \leq 2\sigma^*$ that is crucial to our main results. The schematic idea of the proof is illustrated in Figure 3b). We can also conclude that the minimum of one of the functions σ, ρ also yields a strong, quantitative constraint on the respective other minimum, e.g.,

$$\frac{1}{2}\rho^* \leq \sigma^* \leq \rho^*, \quad (19)$$

meaning that the minimum of σ is bounded from below and above by the minimum of ρ .

Appendix C: The derivative $\partial_{j_{\mathcal{C}}}\rho$ — The minimization of ρ with respect to the current $j_{\mathcal{C}}$ of a fundamental cycle \mathcal{C} can be performed after expressing ρ as an explicit function of the currents j_{ij} . Using the definitions of ρ and F_{ij} , Eqs. (8) and (5) together with $\cosh(\operatorname{asinh}(x)) = \sqrt{x^2 + 1}$, we obtain

$$\rho = \sum_{ij} j_{ij} \operatorname{asinh} \frac{j_{ij}}{2\omega_{ij}} - 2\omega_{ij} \left(\sqrt{\frac{j_{ij}^2}{(2\omega_{ij})^2} + 1} - 1 \right).$$

Applying the derivative $\partial_{j_{\mathcal{C}}}$ as defined in (16) yields

$$\begin{aligned} \partial_{j_{\mathcal{C}}}\rho &= \frac{1}{2} \sum_{ij} \chi_{ij}^{\mathcal{C}} \partial_{j_{ij}} \rho \\ &= \sum_{ij} \chi_{ij}^{\mathcal{C}} \left(\operatorname{asinh} \frac{j_{ij}}{2\omega_{ij}} + \frac{j_{ij}}{\sqrt{j_{ij}^2 + 4\omega_{ij}^2}} - \frac{j_{ij}}{\sqrt{j_{ij}^2 + 4\omega_{ij}^2}} \right) \\ &= \frac{1}{2} \sum_{ij} \chi_{ij}^{\mathcal{C}} F_{ij} = \sum_{(ij) \in \mathcal{C}} F_{ij}. \end{aligned}$$

In passing to the third line, we have again used Eq. (5). The result corresponds to Eq. (13) in the main text.

Appendix D: Optimal vs. conservative current in the unicyclic model— For the model introduced in Fig. 2a), the solutions for $j_{\mathcal{C}}$ that indicate conservative and optimal transport can be characterized and compared explicitly. The optimal current $j_{\mathcal{C}}^*$ is obtained by minimizing Eq. (12), i.e., it solves $\partial\sigma/\partial j_{\mathcal{C}} = 0$, which can be recast as

$$f(j_{\mathcal{C}}^*) = f([J - j_{\mathcal{C}}^*]/e^{-E_b})/(N - 1) \quad (20)$$

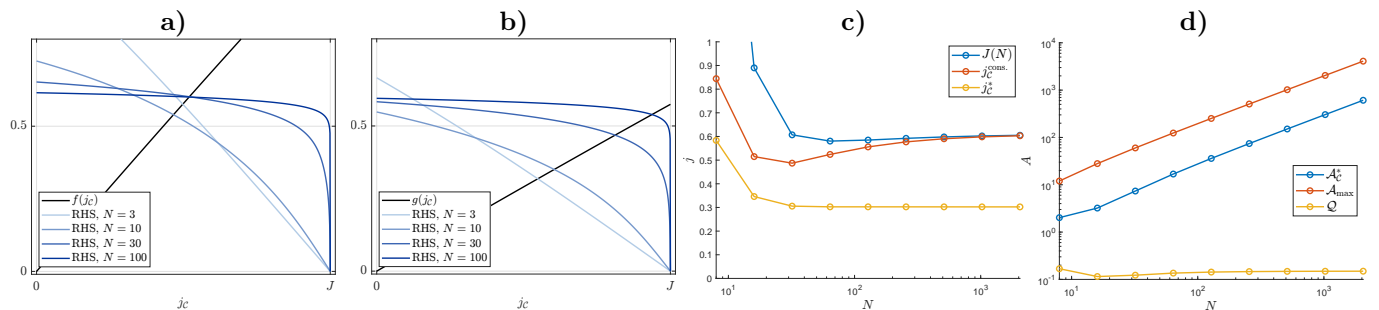


FIG. 4. a) and b) A graphical solution of the transcendent equations (20) and (21). The left-hand side of each equation is depicted as a black solid curve, whereas the right-hand sides are depicted in shades of blue for different values of N , $E_b = NE_0$, $E_0 = 0.3$ and $J = 0.5824$. The abscissa of the intersection of the blue and black curve give the respective value of j_C^* and $j_C^{\text{cons.}}$ in panel a) and b), respectively. c) The numerically optimized $J(N)$ as a function of N for $E_0 = 0.3$ (parameters identical to the purple curve in Fig. 2 b)). The conservative and optimal current are also depicted as functions of N for the same parameters. d) Unlike the conservative solution, the optimal solution j_C^* features a nonzero cycle affinity \mathcal{A}_C^* . Its absolute value for the previous set of parameters is compared to the theoretical upper bound $\mathcal{A}_C^* \leq \mathcal{A}_{\text{max}}(N) = 2(N-2)$ (see Eq. (22) and Ref. [28]). In addition, the quality factor $\mathcal{Q} = \mathcal{A}_C^*/[2(N-2)]$ is shown, which remains roughly constant across all scales of N .

for $f(x) = 2 \operatorname{asinh}(x/2) + 2x/\sqrt{x^2+4}$. A similar transcendent equation for the conservative current $j_C^{\text{cons.}}$ is obtained from the condition of vanishing affinity $\mathcal{A}_C = \sum_{\mathcal{C}} \phi_{ij} = 0$ (cf. Eq. (7)) or, equivalently,

$$g(j_C^{\text{cons.}}) = g([J - j_C^{\text{cons.}}]/e^{-E_b})/(N-1) \quad (21)$$

with $g(x) = 2 \operatorname{asinh}(x/2)$ satisfying $g(x) \leq f(x) \leq 2g(x)$ for $x \geq 0$. This sequence of inequalities can be seen as a differentiated version of the related bounds $\rho \leq \sigma \leq 2\rho$.

A visualization of the transcendent equations (20) and (21) and their solutions j_C^* and $j_C^{\text{cons.}}$ is depicted in Fig. 4 a) and b), respectively, for various values of N and $E_b = NE_0$, with $E_0 = 0.3$ and $J = 0.5824$. As N increases, the conservative solution $j_C^{\text{cons.}}$ approaches J , whereas j_C^* remains roughly centered at around $\simeq J/2$. The observation that $j_C^{\text{cons.}}/j_C^*$ seems to approach a factor of 2 for large N can be understood heuristically from the scaling $f(x) \approx 2g(x)$ for small x , which causes the black curves in Fig. 4 a), b) to appear almost linear with slopes that differ by a factor of 2. As illustrated in Fig. 4 c) this general behavior can be confirmed for higher values of N as well. In this figure, $J(N)$ is not constant but chosen as the optimized value that was also used in Fig. 2 b) for $E_0 = 0.3$. In addition, the currents j_C^* and $j_C^{\text{cons.}}$ are shown as function of N . We note that the currents appear asymptotically constant for large N , which provides an a-posteriori justification for the additional $1/N$ -scaling in these currents compared to the bare probability flow.

As pointed out above, nonconservative driving can only show significant improvement over conservative driving far from equilibrium. This distance to equilibrium can either be characterized in terms of the entropy production rate, as discussed above, or by characterizing the cycle affinity \mathcal{A}_C^* of the optimal solution. Starting from

Eq. (6), the calculation

$$|\mathcal{A}_C^*|/2 = \left| \sum_{(ij) \in \mathcal{C}} F_{ij}/2 \right| = \left| - \sum_{(ij) \in \mathcal{C}} \tanh(F_{ij}/2) \right| \leq N \quad (22)$$

together with the bound $|\tanh x| \leq 1$ for arbitrary x reveals that \mathcal{A}_C^* can grow at most linearly in N . The bound can be slightly improved to $\mathcal{A}_C^* \leq \mathcal{A}_{\text{max}}(N) = 2(N-2)$, as proved in Ref. [28]. In Fig. 4 b) we compare the total affinity \mathcal{A}_C^* in our model as a function of N to the general upper bound. Although \mathcal{A}_C^* does not saturate the bound in any regime, it follows the same linear scaling as a function of N , leading to quality factors $\mathcal{Q} = \mathcal{A}_C^*/[2(N-2)]$ of order 10^{-1} that are mostly independent of N . This finding allows several interesting insights.

First, it confirms that the linear scaling of the affinity bound of Eq. (22) and Ref. [28] as a function of N is already optimal and cannot be improved further. Second, an $N \rightarrow \infty$ -limit of this transport problem is singular in the sense that it does not reduce to the well-known optimal transport problem in overdamped Langevin dynamics, in which the optimal solution can be achieved via conservative forces and therefore has vanishing affinity. Third, as the transport problem is parametrized via $J/N = \dot{p}_2 = -\dot{p}_1$ with J roughly asymptotically constant for large N , the involved currents scale with $1/N$ as well. Therefore, a total affinity that scales proportionally with N is consistent with a total entropy production rate of order 1 without any asymptotic scaling in N and hence also with the delicate result that optimal can improve over conservative driving by a constant factor that is independent of N .